

Quantum control of the dissociation of LiH molecules with two intense laser pulses

Rong Wang and Ying-Yu Niu ^{*}*School of Science, Dalian Jiaotong University, Dalian 116028, China*

(Received 24 March 2020; revised 14 June 2020; accepted 9 July 2020; published 28 July 2020)

The dissociation dynamics of LiH molecules induced by two overlapping femtosecond pulses is investigated based on the time-dependent quantum wave packet method. The first pulse induces population transfer from the ground state $X^1\Sigma^+$ to the excited state $A^1\Sigma^+$ which is coupled with the repulsive state $B^1\Pi$ and the state $X^1\Sigma^+$ by the second pulse. The two products Li($2p$) and Li($2s$) can be obtained via the ladder and Λ transitions, respectively, and the branching ratio of the products can be controlled by varying the second pulse frequency $\hbar\omega_2$. The choice of the intermediate state can affect the dissociation probability and angular distribution of fragments. As the second pulse intensity is increased, more products occur in other directions besides the directions $\theta = 0^\circ$ and 180° . The delay time of two pulses also has influence on the angular distribution.

DOI: [10.1103/PhysRevA.102.013113](https://doi.org/10.1103/PhysRevA.102.013113)

I. INTRODUCTION

Manipulation of molecular reaction processes with laser fields has received much attention in photophysics and photochemistry. With intense laser pulses, photoionization and photodissociation can take place, in which molecular population in bound states is transferred to continuum states, and many interesting phenomena were observed, such as high-order harmonic generation [1,2], above-threshold ionization and dissociation [3,4], Coulomb explosion [5,6], alignment or orientation of molecules [7,8], and control of the photofragment branching ratio [9,10]. Most of these phenomena can be controlled by varying the parameters of laser pulses.

In the processes of dissociation and ionization, an initial electronic state is coupled with one or more final electronic states by the laser field and the molecular population in the initial state can be induced to different states which correspond to different products. Many approaches are proposed to control the angular distribution and branching ratio of products in these final states. Brumer and Shapiro [11,12] employed two harmonic pulses to control dissociation processes. In this method, the direction and probability of products depend on the relative phase of the two pulses [13–15]. Yang and Cong [16], and Han *et al.* [17] used wave packet interference to control the dissociation probability through different channels in two femtosecond pulses. Csehi *et al.* [18] investigated the effect of natural nonadiabatic phenomena on the dissociation process of NaI molecules. Nikodem *et al.* [19] demonstrated spatial and temporal control of products of LiH using a single ultrashort one-cycle pulse. Chamakhi *et al.* [20] explored the control of photoelectron angular distributions by using the delay time of two ultrashort pulses.

In most of the photodissociation cases, the population is induced from a bound ground state to multiple repulsive states to obtain different products. Because there is only a small

energy gap between the ground and repulsive states in the asymptotic region, part of the molecules can be dissociated through the ground state [21–23]. For the LiH molecule, the bound state $A^1\Sigma^+$ and the repulsive state $B^1\Pi$ adjacent to the ground state $X^1\Sigma^+$ and the dissociation energy of the ground state is far away from those of the two excited states, as shown in Fig. 1. As molecular population in the ground state is transferred to the repulsive state, the LiH molecules can be dissociated to two atoms Li($2p$) + H($1s$) and the dissociation in the ground state cannot take place. If the molecules are excited to the state $A^1\Sigma^+$ by the first pulse and then coupled to the states $X^1\Sigma^+$ and $B^1\Pi$ by the second pulse, the dissociation reaction can be achieved in these two electronic states. The corresponding process is depicted in Fig. 1. Moreover, our results show that, comparing with the dissociation $X^1\Sigma^+ \rightarrow B^1\Pi$, products can be distributed in more directions in the dissociation $A^1\Sigma^+ \rightarrow B^1\Pi$.

In this paper, we employ two overlapping femtosecond pulses to control the dissociation of LiH molecules. The rovibrational level in the bound excited state $A^1\Sigma^+$ is chosen as the intermediate state and the products Li($2p$) and Li($2s$) are obtained through the ladder transition $X^1\Sigma^+ \rightarrow A^1\Sigma^+ \rightarrow B^1\Pi$ and Λ transition $X^1\Sigma^+ \rightarrow A^1\Sigma^+ \rightarrow X^1\Sigma^+$, respectively. By varying the second pulse frequency, the product probability dissociated from the states $X^1\Sigma^+$ and $B^1\Pi$ can be controlled. The effects of second pulse intensity and delay time on the branch ratio and angular distribution are examined, and the relation between dissociation process and the intermediate state is discussed in detail.

II. THEORETICAL METHOD

In our model, dissociation takes place in three electronic states, the ground state $X^1\Sigma^+$ and the two excited states $A^1\Sigma^+$ and $B^1\Pi$. For convenience, the three states are abbreviated to $|X\rangle$, $|A\rangle$, and $|B\rangle$, respectively. In the two femtosecond laser pulses, the LiH molecules can be dissociated to three

^{*}niuyy@djtu.edu.cn

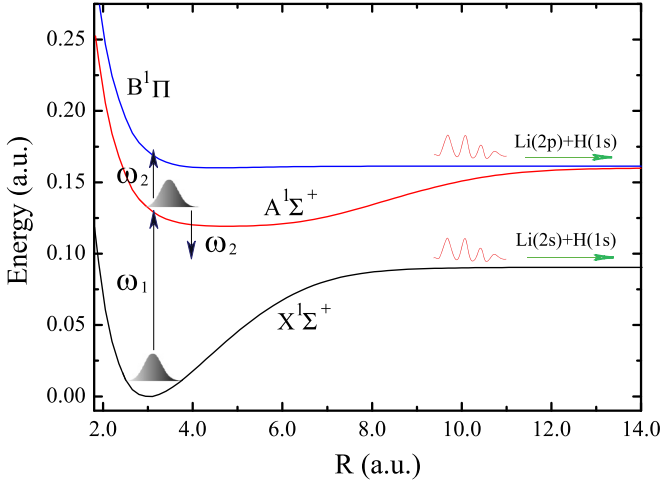


FIG. 1. The potential energy curves of the LiH molecule and dissociation process steered by two intense pulses.

$$i\hbar \frac{\partial}{\partial t} \begin{pmatrix} \Psi_X \\ \Psi_A \\ \Psi_B \end{pmatrix} = \begin{pmatrix} H'_X + U_X + W_{XX} & W_{XA} & W_{XB} \\ W_{AX} & H'_A + U_A + W_{AA} & W_{AB} \\ W_{BX} & W_{BA} & H'_B + U_B + W_{BB} \end{pmatrix} \begin{pmatrix} \Psi_X \\ \Psi_A \\ \Psi_B \end{pmatrix}, \quad (3)$$

with

$$H'_i = T_R + T_\theta, \quad i = X, A, B, \quad (4)$$

where T_R and T_θ are the kinetic-energy terms of the molecular Hamiltonian [24], and U_i is the potential energy function. The interaction W_{ik} of laser pulses and molecules can be written as

$$W_{ik} = -\mu_{ik}(R) \cos \theta \varepsilon(t), \quad i, k = X, A, B, \quad (5)$$

where the functions $\mu_{ik}(R)$ are the transition dipole moment ($i \neq k$) and the permanent dipole moment ($i = k$), respectively, and θ is the angle between the laser field direction and the molecular axis. The data of $U_i(R)$ and $\mu_{ik}(R)$ are obtained from Ref. [25]. The electric field $\varepsilon(t)$ includes two laser pulses which are given by [26,27]

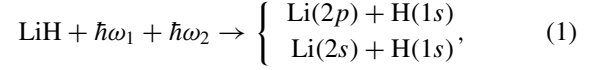
$$\varepsilon(t) = \varepsilon_1 \sin^2 \left[\frac{\pi(t-t_1)}{\tau_1} \right] \cos[\omega_1(t-t_1) + \phi_1] + \varepsilon_2 \sin^2 \left[\frac{\pi(t-t_2)}{\tau_2} \right] \cos[\omega_2(t-t_2) + \phi_2], \quad (6)$$

where τ_n , ω_n , t_n , and ϕ_n ($n = 1, 2$) denote duration, frequency, start time, and initial phase of the n th pulse, respectively. ε_n is the pulse amplitude corresponding to peak intensity $I_n = \frac{1}{2} c \varepsilon_0 \varepsilon_n^2$. The delay time of two-pulse central time is $\Delta t = (t_2 + \tau_2/2) - (t_1 + \tau_1/2)$. The start time t_1 and initial phases of two pulses are set as 0.

The split operator method [28] is used here to solve Eq. (2) and the wave function $\Psi(R, \theta, t)$ with time propagation can be obtained. An absorption potential $U_{abs}(R)$ is used to avoid reflection of the wave packet at the boundary [29],

$$\psi_i(R, \theta, t) = U_{abs}(R) \Psi_i(R, \theta, t), \quad i = X, A, B, \quad (7)$$

products,



where $\text{Li}(2p)$ and $\text{H}(1s)$ are derived from the two excited states and $\text{Li}(2s)$ and $\text{H}(1s)$ correspond to the ground state.

In the Born-Oppenheimer approximation, the dynamics processes of photodissociation can be obtained by solving the time-dependent Schrödinger equation,

$$i\hbar \frac{\partial}{\partial t} \Psi(R, \theta, t) = \hat{H} \Psi(R, \theta, t), \quad (2)$$

where $\Psi(R, \theta, t)$ is the molecular wave function. Because the linearly polarized laser pulses are used, the azimuthal angle φ is ignored. Equation (2) can be expressed as the coupled matrix equation:

with

$$U_{abs}(R) = \frac{1}{1 + \exp[\eta(R - R_a)]}, \quad (8)$$

where R_a is the central position of the absorption potential region, and the parameter η determines the rate of decay.

The angle-dependent outgoing flux at $R = R_0$ is defined as [17,30]

$$F_i(\theta, t) = \frac{\hbar}{m} \text{Im} \left[\psi_i^*(R_0, \theta, t) \frac{\partial}{\partial R} \psi_i(R, \theta, t) \Big|_{R_0} \right], \quad i = X, A, B, \quad (9)$$

where m is the reduced mass. The angular distribution of the i th channel can be written as

$$P_i(\theta) = \int_0^{t'} F_i(\theta, t) dt. \quad (10)$$

The value of $P_i(\theta)$ depends on the number of the angular grid points. The normalized dissociation probability of the i th state can be obtained by

$$P'_i = \int_0^\pi P_i(\theta) \sin \theta d\theta. \quad (11)$$

The time t' can be obtained as the dissociation probability P'_i reaches a constant value. The final population of the vibrational level in the i th state can be expressed as

$$P_i^\nu = \sum_{J=0}^{J_{\max}} |\langle \nu, J | \psi_i(R, \theta, t') \rangle|^2, \quad (12)$$

where ν and J are the vibrational and rotational quantum numbers, respectively, and $|\nu, J\rangle$ is the eigenfunction of rovibrational level.

The energy distribution of dissociation fragments of the i th state is calculated by

$$Q_i(E_n) = \int_0^\pi \sin \theta d\theta \int_0^{t'} F'_i(k_n, \theta, t) dt, \quad (13)$$

with

$$F'_i(k_n, \theta, t) = \text{Re} \left\{ \psi_i^*(R_0, \theta, t) \frac{2\pi(n-1)}{m(R_{\max} - R_{\min})} \times \exp[2i\pi(n-1)(n_0-1)/N] \psi'_i(k_n, \theta, t) \right\}, \quad (14)$$

where $E_n = k_n^2/2m$ is the kinetic energy, $(R_{\max} - R_{\min})$ is the range of radial part R , and n_0 is the number of grid points corresponding to R_0 . The wave function $\psi'_i(k_n, \theta, t)$ in momentum space is obtained by a discrete Fourier transform of $\psi_i(R, \theta, t)$.

The branching ratio of $\text{Li}(2s)$ is defined as

$$\Gamma \left(\frac{\text{Li}(2s)}{\text{Li}(2s) + \text{Li}(2p)} \right) = \frac{P'_X}{P'_X + P'_A + P'_B} = \frac{P'_{2s}}{P'_{2s} + P'_{2p}}, \quad (15)$$

where P'_{2s} and P'_{2p} are the dissociation probabilities of $\text{Li}(2s)$ and $\text{Li}(2p)$, respectively.

III. RESULTS AND DISCUSSIONS

In our calculation, the radial part R is from 1.2 to 65.0 a.u. with the 2048-point Fourier grid. The DVR grid points of angular degrees are 60-Gauss-Legendre quadrature points. The parameters η and R_0 in Eq. (8) are chosen as 6.0 and 55.0 a.u., respectively, and the value of R_0 in Eq. (9) is set as 42.0 a.u.. The rovibrational level $|\nu = 0, J = 0\rangle_X$ in the state $|X\rangle$ is chosen as the initial state and the two overlapping pulses with duration 100 fs are employed to control the dissociation.

In a ladder transition, molecules are induced from the ground states $|X\rangle$ to the intermediate state $|A\rangle$ by the first pulse and then to the repulsive state $|B\rangle$ by the second pulse. For choosing a proper vibrational level in the state $|A\rangle$ as the intermediate state, the Franck-Condon factors F between the vibrational level $\nu = 0$ in the state $|X\rangle$ and different vibrational levels ν in the state $|A\rangle$ are calculated in Fig. 2(a). When the vibrational level is $\nu = 7$ in the state $|A\rangle$, the corresponding Franck-Condon factor reaches the maximum value. Although the two dissociations $|X\rangle \rightarrow |B\rangle$ and $|A\rangle \rightarrow |B\rangle$ produce the same products $\text{Li}(2p) + \text{H}(1s)$, their angular distributions may different because of the different structures of potential energy curves in the states $|X\rangle$ and $|A\rangle$. The processes of two dissociations are interpreted in terms of the light-dressed potential [31], as shown in Figs. 2(b)–2(e). The left-hand panel is for the transition $|X\rangle \rightarrow |B\rangle$ with the frequency $34\,788\text{ cm}^{-1}$ which corresponds to the energy gap ΔE_{XB} between the eigenenergy of $|\nu = 0, J = 0\rangle_X$ and the dissociation energy of $|B\rangle$, and the right-hand panel is for the transition $|A\rangle \rightarrow |B\rangle$ with the frequency 6626 cm^{-1} which corresponds to the energy gap ΔE_{AB} between the eigenenergy of $|\nu = 7, J = 1\rangle_A$ and the dissociation energy of $|B\rangle$. In Fig. 2(d), there is a large peak at $\theta = 90^\circ$ and most of the dissociation wave packet moves towards $\theta = 0^\circ$ and 180° . For the dissociation $|A\rangle \rightarrow |B\rangle$, the adiabatic surface only has a

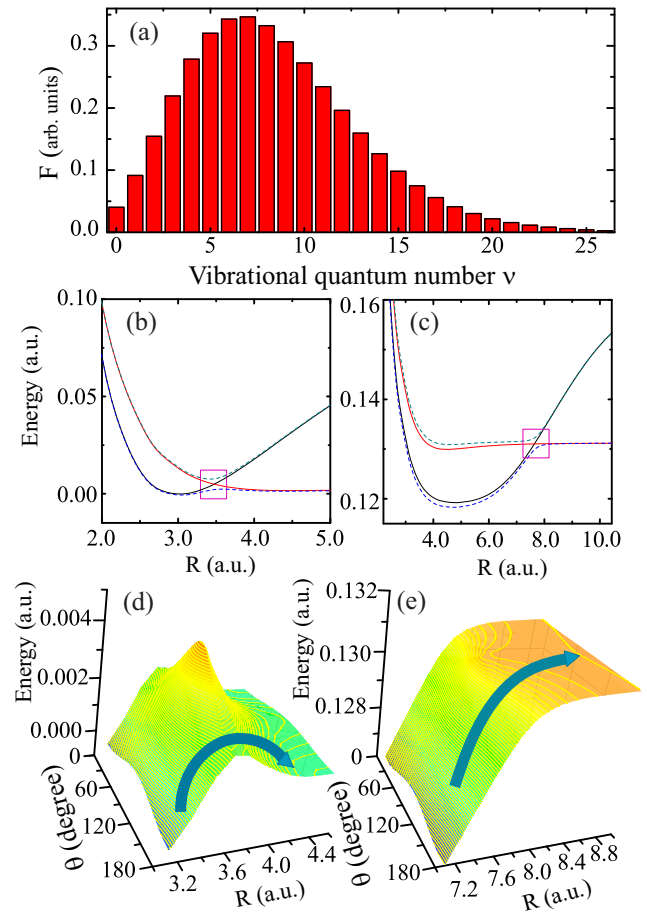


FIG. 2. (a) The Franck-Condon factors F between the vibrational level $\nu = 0$ in the state $|X\rangle$ and different vibrational levels ν in the state $|A\rangle$. (b) and (c) The diabatic (solid lines) and adiabatic (dashed lines) light-dressed potential curves with $I = 5.6 \times 10^{11}\text{ W/cm}^2$. The left-hand panel is for the states $|X\rangle$ and $|B\rangle$ with the frequency $34\,788\text{ cm}^{-1}$ and the right-hand panel is for the states $|A\rangle$ and $|B\rangle$ with the frequency 6626 cm^{-1} . (d) and (e) Three-dimensional graphs of adiabatic surfaces in the regions of rectangular boxes in Figs. 2(b) and 2(c), respectively. The arrows give an illustration of the moving direction of the wave packet.

small peak at $\theta = 90^\circ$ in Fig. 2(e). This means that it is easier for the products in the transition $|A\rangle \rightarrow |B\rangle$ to occur in the other directions besides $\theta = 0^\circ$ and 180° .

The angular distributions for the dissociations $|X\rangle \rightarrow |B\rangle$ and $|A\rangle \rightarrow |B\rangle$ induced by one pulse are shown in Fig. 3, in which the rovibrational levels $|\nu = 0, J = 0\rangle_X$ and $|\nu = 7, J = 1\rangle_A$ are chosen as the initial states, respectively and the difference value between $\hbar\omega$ and ΔE_{XB} in Fig. 3(a) is the same as that between $\hbar\omega$ and ΔE_{AB} in Fig. 3(b). In Fig. 3(a), the value of P_B is increased with the increase of intensity I . All of products are distributed in the regions $\theta < 75^\circ$ and $\theta > 105^\circ$ and the maximum value of P_B is occurred at 0° and 180° . When the initial state is $|\nu = 7, J = 1\rangle_A$, the maximum value of P_B is also at 0° and 180° in Fig. 3(b). The maximum value of P_B in Fig. 2(b) is larger than that in Fig. 3(a). That is to say, more products can be obtained in the transition $|A\rangle \rightarrow |B\rangle$. There are obvious fragments occurred at near 90° for $I > 4.0 \times 10^{11}\text{ W/cm}^2$ in Fig. 3(b). We can see from Fig. 3

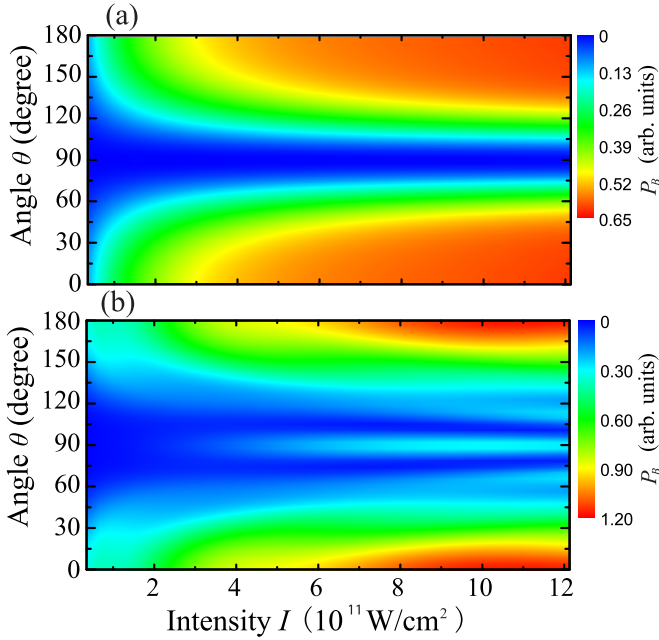


FIG. 3. The angular distributions of products as a function of intensity I in one pulse. (a) The initial state is $|\nu = 0, J = 0\rangle_X$ in the state $|X\rangle$. The parameters of pulse are chosen as $\tau = 100$ fs and $\hbar\omega = 36543$ cm^{-1} . (b) The initial state is $|\nu = 7, J = 1\rangle_A$ in the state $|A\rangle$. The parameters of pulse are chosen as $\tau = 100$ fs and $\hbar\omega = 8381$ cm^{-1} .

that the angular distribution for the transition $|A\rangle \rightarrow |B\rangle$ is different from that for the transition $|X\rangle \rightarrow |B\rangle$. Moreover, our calculated results show that some products $\text{Li}(2s)$ occurred in the state $|X\rangle$ with the initial state $|\nu = 7, J = 1\rangle_A$, and these products cannot be found with the initial state $|\nu = 0, J = 0\rangle_X$.

It can be seen from Fig. 3 that the angular distribution region of products $\text{Li}(2p)$ for the transition $|A\rangle \rightarrow |B\rangle$ is larger than that for the transition $|X\rangle \rightarrow |B\rangle$. As a dissociation is achieved via the intermediate state $|A\rangle$ in the ladder transition $|X\rangle \rightarrow |A\rangle \rightarrow |B\rangle$, the angular distribution of fragments will be similar with that in Fig. 3(b). Figure 4 shows the ladder transition with the intermediate state $|\nu = 7, J = 1\rangle_A$ induced by two overlapping pulses, in which the frequency of the second pulse is the same as that in Fig. 3(b). When the intensity I_2 is 5.6×10^{11} W/cm^2 , the curve of energy distribution shows only one peak at $1\hbar\omega_2$ in Fig. 4(a). This means that the dissociation is taken place via one-photon transition. In Fig. 4(b), nearly all of the products are derived from the state $|B\rangle$ and the dissociation probabilities in the states $|X\rangle$ and $|A\rangle$ are very small (<0.02). The probability of products $\text{Li}(2p)$ is increased with the increase of intensity I_2 . When the intensity of the second pulse is 5.6×10^{11} W/cm^2 , the value of P'_B is 0.52. As the intensity I_2 is decreased to 5.6×10^{10} W/cm^2 , the dissociation probability is only 0.15. Numico *et al.* [31] demonstrated that photofragments in the $\theta = 90^\circ$ direction can be enhanced by the high intensity. The variation of angular distribution for different intensities I_2 is shown in Fig. 4(c). When the intensity I_2 is 5.6×10^{10} W/cm^2 , the value of P_{2p} is 0 at $\theta = 90^\circ$ and most of the products are distributed in the regions $\theta < 30^\circ$ and $\theta > 150^\circ$. For $I_2 = 2.6 \times 10^{11}$ W/cm^2 ,

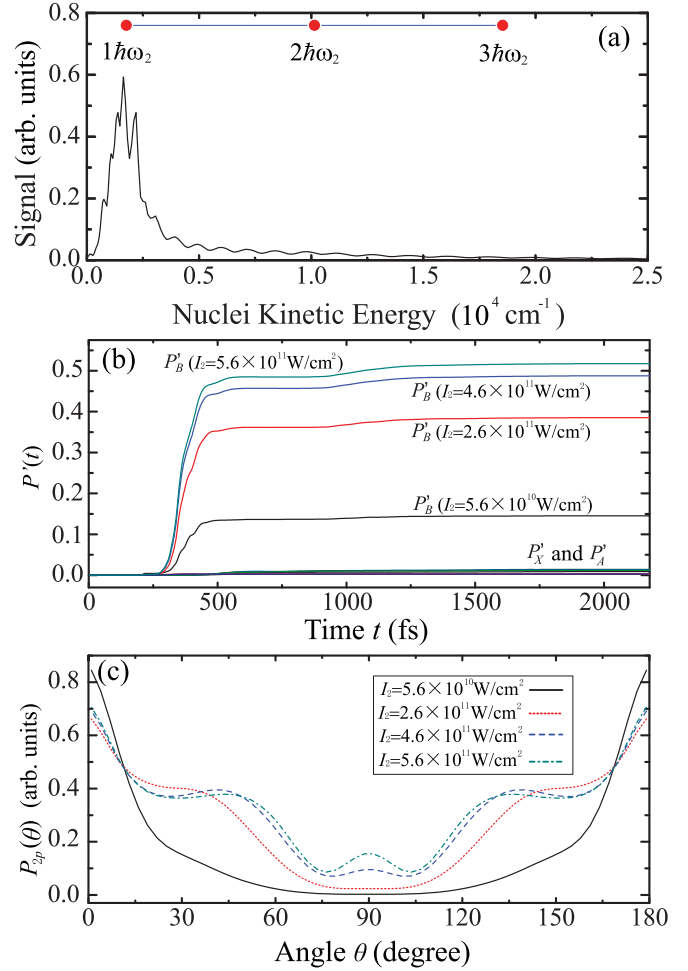


FIG. 4. The dissociation through the ladder transition with the intermediate state $|\nu = 7, J = 1\rangle_A$. (a) The energy distribution of fragments for $I_2 = 5.6 \times 10^{11}$ W/cm^2 . (b) The dissociation probabilities P' for different intensities I_2 . (c) The angular distributions of products $\text{Li}(2p)$ ($P_{2p} = P_A + P_B$) for different intensities I_2 . The pulse parameters are $\hbar\omega_1 = 28162$ cm^{-1} , $\hbar\omega_2 = 8381$ cm^{-1} , $\tau_1 = \tau_2 = 100$ fs, $I_1 = 7.5 \times 10^{12}$ W/cm^2 , and $\Delta t = 24.2$ fs (1000 a.u.), respectively.

the value of P_{2p} is increased at $\theta = 45^\circ$ and 135° . When the intensity I_2 is increased to 5.6×10^{11} W/cm^2 , the curve of P_{2p} shows three obvious peaks at $\theta = 45^\circ$, 90° , and 135° . With the increase of the second pulse intensity, the probabilities of products occurring at these three degrees are increased.

When the intensity I_2 is chosen as 5.6×10^{11} W/cm^2 , the dissociation probability and angular distribution have obvious differences for different intermediate states. Figure 5 shows the dissociations for four intermediate states, in which the first pulse frequency $\hbar\omega_1$ is equal to the resonant frequency between the initial and intermediate states and the sum of two-pulse frequencies is the same as that in Fig. 4. In Fig. 2(a), the Franck-Condon factor for $\nu = 7$ reaches the maximum value and the values of F for $\nu = 3$ and $\nu = 12$ are nearly the same. When the rovibrational level $|\nu = 7, J = 1\rangle_A$ is chosen as the intermediate state, the dissociation probability is larger than those of the other intermediate states in Fig. 5(a). The probability of products for $|\nu = 3, J = 1\rangle_A$ is nearly equal to

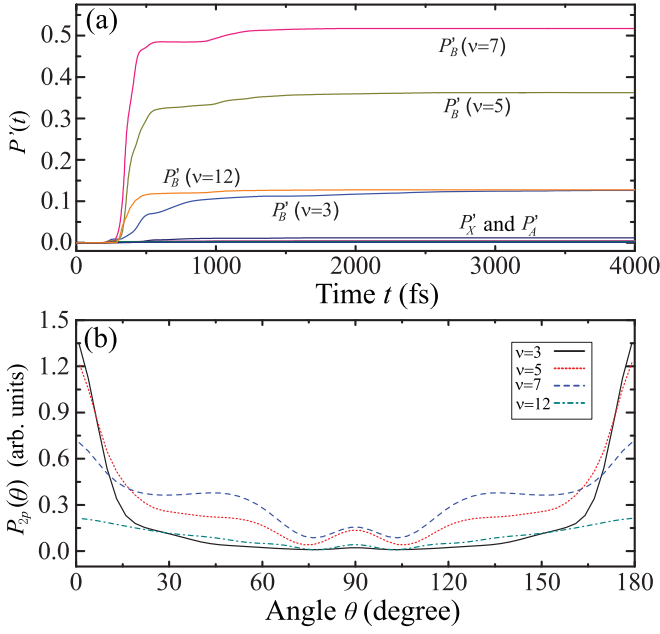


FIG. 5. (a) The dissociation probabilities P' for different intermediate states. (b) The angular distributions P_{2p} for different intermediate states. The pulse frequencies are $\hbar\omega_1 = 26\,646\text{ cm}^{-1}$ and $\hbar\omega_2 = 9\,897\text{ cm}^{-1}$ for $\nu = 3$, $\hbar\omega_1 = 27\,385\text{ cm}^{-1}$ and $\hbar\omega_2 = 9\,158\text{ cm}^{-1}$ for $\nu = 5$, $\hbar\omega_1 = 28\,162\text{ cm}^{-1}$ and $\hbar\omega_2 = 8\,381\text{ cm}^{-1}$ for $\nu = 7$, and $\hbar\omega_1 = 30\,150\text{ cm}^{-1}$ and $\hbar\omega_2 = 6\,393\text{ cm}^{-1}$ for $\nu = 12$, respectively, and the other parameters of two pulses are chosen as $\tau_1 = \tau_2 = 100\text{ fs}$, $I_1 = 7.5 \times 10^{12}\text{ W/cm}^2$, $I_2 = 5.6 \times 10^{11}\text{ W/cm}^2$, $\Delta t = 24.2\text{ fs}$.

that for $|\nu = 12, J = 1\rangle_A$. It can be seen from Figs. 2(a) and 5(a) that the variations of P'_B and F with the vibrational level ν in the state $|A\rangle$ are similar and the transition probability between the initial and intermediate states can determine the final dissociation probability. When the intermediate state is $|\nu = 3, J = 1\rangle_A$, there are no products at $\theta = 90^\circ$ and most of the products are distributed in the regions $\theta < 30^\circ$ and $\theta > 150^\circ$, as shown in Fig. 5(b). For the intermediate state $|\nu = 5, J = 1\rangle_A$, there is a peak at $\theta = 90^\circ$ in the curve of P_{2p} . The values of P_{2p} for $|\nu = 7, J = 1\rangle_A$ at $\theta = 45^\circ, 90^\circ$, and 135° are increased. We can see from Figs. 5(a) and 5(b) that more fragments are distributed in the region $30^\circ < \theta < 150^\circ$ with the increase of dissociation probability. Besides the dissociation probability, the angular distribution of fragments depends on the vibrational quantum number ν of the intermediate state. For the intermediate states $|\nu = 3, J = 1\rangle_A$ and $|\nu = 12, J = 1\rangle_A$, their dissociation probabilities are nearly the same, but the values of P_{2p} for $|\nu = 12, J = 1\rangle_A$ at $\theta = 0^\circ$ and 180° are smaller than those for $|\nu = 3, J = 1\rangle_A$. It can be seen from Fig. 5(b) that the values of P_{2p} at $\theta = 0^\circ$ and 180° are decreased with the increase of vibrational level ν .

In the dissociation process, the first pulse can induce molecules transferring to multiple intermediate states because of its large bandwidth. Figure 6(c) shows the final population distribution in the state $|A\rangle$ induced by only the first pulse with the parameters for $\nu = 12$. The population is transferred to six vibrational levels (from $\nu = 10$ to $\nu = 15$) at the end of the first pulse. That is to say, the dissociation is achieved

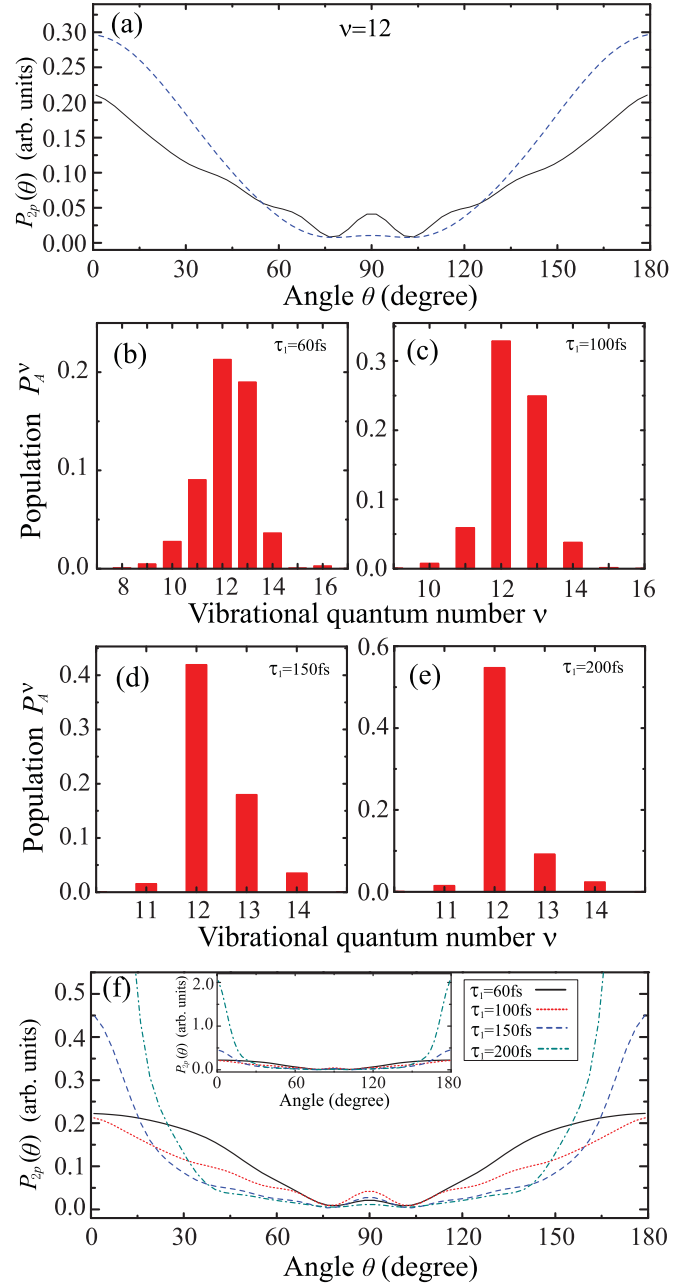


FIG. 6. (a) The angular distributions for different initial states. The dashed curve is for the initial state $|\nu = 12, J = 1\rangle_A$ in only the second pulse and the solid curve is for the initial state $|\nu = 0, J = 0\rangle_X$ in two pulses. (b)–(e) The final population P_A^ν in the state $|A\rangle$ for different durations τ_1 in only the first pulse. (f) The angular distributions for different durations τ_1 in two pulses. The whole angular distribution for $\tau_1 = 200\text{ fs}$ is shown in the inset. The pulse parameters are the same as those for $\nu = 12$ in Fig. 5.

via multiple intermediate states in the transition $|X\rangle \rightarrow |A\rangle \rightarrow |B\rangle$. The corresponding curve of angular distribution shows a peak at $\theta = 90^\circ$ in Fig. 6(a). As the rovibrational level $|\nu = 12, J = 1\rangle_A$ is chosen as the initial state, there are no products at $\theta = 90^\circ$. This means that the angular distribution is affected by the number of intermediate states which is determined by the duration of the first pulse. When the duration τ_1 is 200 fs, the population stays in four vibrational levels in Fig. 6(e), and

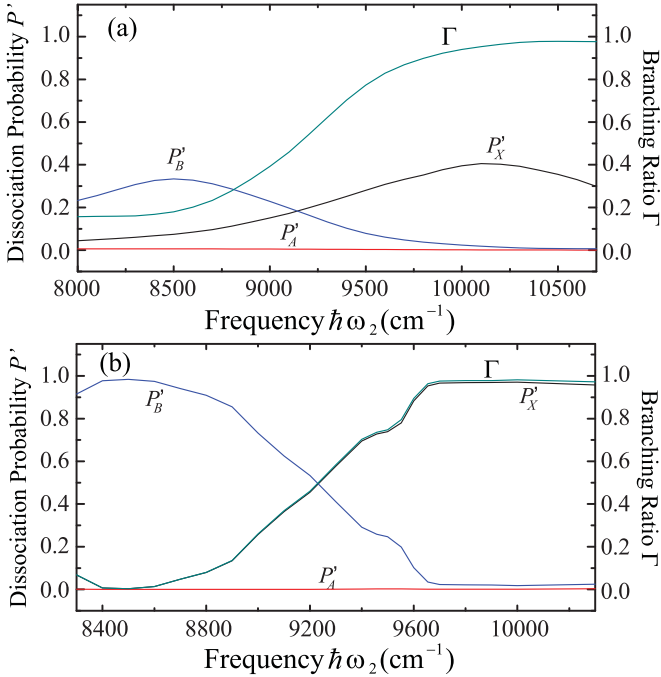


FIG. 7. The dissociation probability P' and branching ratio Γ as a function of the second pulse frequency $\hbar\omega_2$. (a) The dissociation in two-fs pulses. The first pulse frequency is $\hbar\omega_1 = 30150 \text{ cm}^{-1}$ and the other parameters of two pulses are the same as those in Fig. 5. (b) The dissociation in two-ps pulses. The pulse parameters are $\hbar\omega_1 = 30150 \text{ cm}^{-1}$, $\tau_1 = \tau_2 = 10 \text{ ps}$, $I_1 = 7.5 \times 10^8 \text{ W/cm}^2$, $I_2 = 2.0 \times 10^{11} \text{ W/cm}^2$, and $\Delta t = 7.26 \text{ ps}$, respectively.

the values of P_{2p} are increased rapidly in the regions $\theta < 45^\circ$ and $\theta > 135^\circ$ in Fig. 6(f). For $\tau_1 = 150 \text{ fs}$, the population ratios of $\nu = 12$ to $\nu = 13$ and to $\nu = 14$ are decreased in Fig. 6(d), and there are some products at $\theta = 90^\circ$ in Fig. 6(f). When the duration is 100 fs and 60 fs, population is transferred to more vibrational levels in Figs. 6(b) and 6(c), and the values of P_{2p} in the regions $\theta < 45^\circ$ and $\theta > 135^\circ$ are reduced in Fig. 6(f). With the decrease of the first pulse duration, more intermediate states take part in a ladder transition and the value of P_{2p} in $45^\circ < \theta < 135^\circ$ is increased, as shown in Figs. 6(b)–6(f).

In the above cases, the dissociation probability from the intermediate state $|\nu = 7, J = 1\rangle_A$ to the state $|X\rangle$ induced by the second pulse is small and about 100% of products are obtained through the ladder transition. As the rovibrational level $|\nu = 12, J = 1\rangle_A$ is chosen as the intermediate state, the probability of products $\text{Li}(2s)$ can be increased and the ladder transition is accompanied by the Λ transition. Figure 7(a) shows the dissociation probability P' and branching ratio Γ by varying the second pulse frequency, in which the first pulse frequency is 30150 cm^{-1} , corresponding to the resonant frequency between the levels $|\nu = 0, J = 0\rangle_X$ and $|\nu = 12, J = 1\rangle_A$. When the frequency $\hbar\omega_2$ is changed from 8000 cm^{-1} to 10500 cm^{-1} , P'_B is increased to the maximum value at 8500 cm^{-1} and then decreased to nearly 0 at 10500 cm^{-1} . For $\hbar\omega_2 < 10100 \text{ cm}^{-1}$, the dissociation probability P'_X through the Λ transition is increased with the increase of $\hbar\omega_2$. As the value of $\hbar\omega_2$ is increased from 10100 cm^{-1} , the second

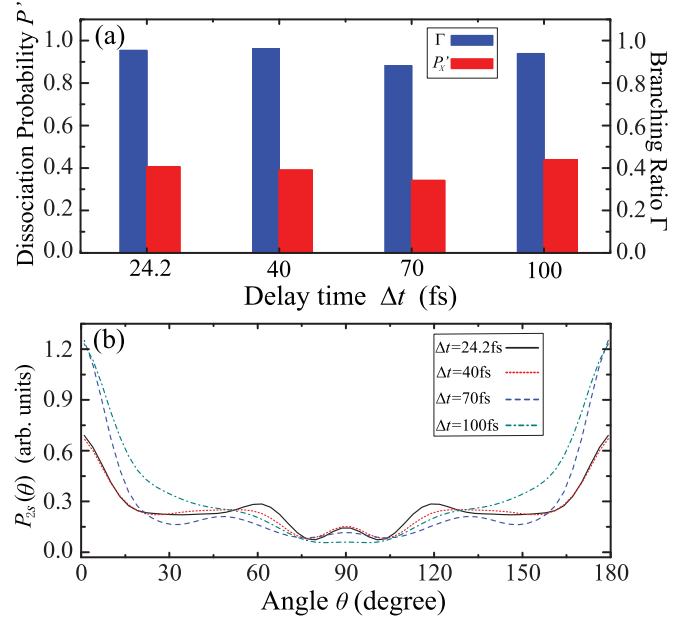


FIG. 8. The dissociation through the Λ transition with the intermediate state $|\nu = 12, J = 1\rangle_A$. (a) The dissociation probability P'_X (red column) and branching ratio Γ (blue column) for different delay times Δt . (b) The angular distribution P_{2s} of products $\text{Li}(2s)$ for different delay times Δt . The second pulse frequency is $\hbar\omega_2 = 10100 \text{ cm}^{-1}$ and the other parameters of two pulses are the same as those in Fig. 7(a).

pulse frequency is close to the energy gap between the level $|\nu = 12, J = 1\rangle_A$ and the dissociation energy of $|X\rangle$. Because the Franck-Condon factors between the intermediate state and the levels near the dissociation energy of $|X\rangle$ are small (< 0.05), the probability of products $\text{Li}(2s)$ is decreased. The branching ratio Γ is increased from 0.16 to 0.98 by varying the second pulse frequency. This means that the frequency $\hbar\omega_2$ can efficiently control the fragment branching ratio. Figure 7(b) shows the dissociation induced by two-ps pulses. Because the durations of two pulses are increased, about 100% of molecules are dissociated and the two curves of Γ and P'_X are nearly overlapped. As the frequency $\hbar\omega_2$ is changed from 8400 cm^{-1} to 10000 cm^{-1} , the branching ratio Γ is increased from 0.003 to 0.98. It can be seen that the scenario of controlling the branching ratio with $\hbar\omega_2$ can be used to both femtosecond and picosecond pulse schemes.

Figure 8 shows the dissociation for different delay times Δt with the intermediate state $|\nu = 12, J = 1\rangle_A$. Because the second pulse frequency is 10100 cm^{-1} , molecules are mainly dissociated through the Λ transition. In Fig. 8(a), the maximum and minimum probabilities of products $\text{Li}(2s)$ are 0.44 at $\Delta t = 100 \text{ fs}$ and 0.34 at $\Delta t = 70 \text{ fs}$, respectively, and the values for all branching ratios Γ are greater than 88%. This means that the delay time of two pulses has a weak influence on the dissociation probability. The delay time can be used to control the angular distribution of products [20]. When the delay time is 100 fs, the second pulse is turned on at the end of the first pulse. The value of P_{2s} is increased from 0.05 to 1.23 as the degree is changed from 90° to 180° and to 0° . For $\Delta t = 70 \text{ fs}$, there are three peaks at $\theta = 45^\circ, 90^\circ,$

and 135° . As the delay time is changed to 40 fs and to 24.2 fs, the values of the three peaks are increased, which leads to the decrease of products at $\theta = 0^\circ$ and 180° . It can be seen that the curves of P_{2s} show obvious oscillation as the two pulses are overlapped ($\Delta t < 100$ fs).

IV. CONCLUSION

In this paper, we have studied the dissociation process of LiH molecules in two laser pulses, in which molecules are dissociated via intermediate states and the products Li($2p$) and Li($2s$) are obtained through the ladder and Λ transitions, respectively. As the rovibrational level $|\nu = 7, J = 1\rangle_A$ is chosen as the intermediate state and the second pulse frequency is near the energy gap between the intermediate state and dissociation energy of $|B\rangle$, nearly all of the products are dissociated from the state $|B\rangle$ through the ladder transition. Besides the directions $\theta = 0^\circ$ and 180° , more products are occurred in the other directions, such as 45° , 90° , and 135° , with the increase of intensity I_2 . The choice of the intermediate state

can affect the dissociation probability which determines the angular distribution of fragments. As the first pulse duration is decreased, molecules are dissociated via more intermediate states and the products distributed in $45^\circ < \theta < 135^\circ$ are increased. With the intermediate state $|\nu = 12, J = 1\rangle_A$, the Λ transition takes place simultaneously with the ladder transition and the branching ratio of products Li($2s$) can be controlled by the second pulse frequency. The angular distribution depends on the delay time of two pulses. As the first pulse is overlapped with the second pulse, the amplitude of oscillation for the curve of angular distribution is increased.

ACKNOWLEDGMENTS

This work is supported by the Natural Science Foundation of Liaoning Province of China (Grant No. 20170540135), the National Natural Science Foundation of China under Grant No. 11347012, and the Scientific Research Fund of Liaoning Provincial Education Department of China (Grant No. JDL2017012).

-
- [1] A. L'Huillier, K. J. Schafer, and K. C. Kulander, *J. Phys. B.* **24**, 3315 (1991).
 - [2] X.-B. Bian and A. D. Bandrauk, *Phys. Rev. Lett.* **113**, 193901 (2014).
 - [3] P. Agostini, F. Fabre, G. Mainfray, G. Petite, and N. K. Rahman, *Phys. Rev. Lett.* **42**, 1127 (1979).
 - [4] N. Suárez, A. Chacón, M. F. Ciappina, B. Wolter, J. Biegert, and M. Lewenstein, *Phys. Rev. A.* **94**, 043423 (2016).
 - [5] A. S. Alnaser, X. M. Tong, T. Osipov, S. Voss, C. M. Maharjan, P. Ranitovic, B. Ulrich, B. Shan, Z. Chang, C. D. Lin *et al.*, *Phys. Rev. Lett.* **93**, 183202 (2004).
 - [6] B. Manschwetus, T. Nubbemeyer, K. Gorling, G. Steinmeyer, U. Eichmann, H. Rottke, and W. Sandner, *Phys. Rev. Lett.* **102**, 113002 (2009).
 - [7] H. Stapelfeldt and T. Seideman, *Rev. Mod. Phys.* **75**, 543 (2003).
 - [8] L. Holmegaard, J. L. Hansen, L. Kalthøj, S. L. Kragh, H. Stapelfeldt, F. Filsinger, J. Küpper, G. Meijer, D. Dimitrovski, M. Abu-samha *et al.*, *Nat. Phys.* **6**, 428 (2010).
 - [9] D. J. Tannor and S. A. Rice, *J. Chem. Phys.* **83**, 5013 (1985).
 - [10] S. Chatterjee, B. Dutta, and S. S. Bhattacharyya, *Phys. Rev. A.* **83**, 063413 (2011).
 - [11] P. Brumer and M. Shapiro, *Chem. Phys. Lett.* **126**, 541 (1986).
 - [12] M. Shapiro, J. W. Hepburn, and P. Brumer, *Chem. Phys. Lett.* **149**, 451 (1988).
 - [13] S.-M. Wang, K.-J. Yuan, Y.-Y. Niu, Y.-C. Han, and S.-L. Cong, *Phys. Rev. A.* **74**, 043406 (2006).
 - [14] H. Ohmura, T. Nakanaga, and M. Tachiya, *Phys. Rev. Lett.* **92**, 113002 (2004).
 - [15] A. D. Bandrauk and S. Chelkowski, *Phys. Rev. Lett.* **84**, 3562 (2000).
 - [16] D. Yang and S.-L. Cong, *Phys. Rev. A.* **84**, 013424 (2011).
 - [17] Y.-C. Han, K.-J. Yuan, W.-H. Hu, T.-M. Yan, and S.-L. Cong, *J. Chem. Phys.* **128**, 134303 (2008).
 - [18] A. Csehi, G. J. Halász, and A. Vibók *Chem. Phys.* **509**, 91 (2018).
 - [19] A. Nikodem, R. D. Levine, and F. Remacle, *Phys. Rev. A.* **95**, 053404 (2017).
 - [20] R. Chamakhi, M. Telmini, O. Atabek, and E. Charron, *Phys. Rev. A.* **100**, 033402 (2019).
 - [21] W. Gao, B.-B. Wang, X.-J. Hu, S. Chai, Y.-C. Han, and J. B. Greenwood, *Phys. Rev. A.* **96**, 013426 (2017).
 - [22] P. A. Orr, I. D. Williams, J. B. Greenwood, I. C. E. Turcu, W. A. Bryan, J. Pedregosa-Gutierrez, and C. W. Walter, *Phys. Rev. Lett.* **98**, 163001 (2007).
 - [23] J. McKenna, A. M. Saylor, F. Anis, B. Gaire, N. G. Johnson, E. Parke, J. J. Hua, H. Mashiko, C. M. Nakamura, E. Moon, Z. Chang, K. D. Carnes, B. D. Esry, and I. Ben-Itzhak, *Phys. Rev. Lett.* **100**, 133001 (2008).
 - [24] R. Wang, Y.-Y. Niu, M.-H. Qiu, and Y.-C. Han, *Phys. Rev. A.* **91**, 013401 (2015).
 - [25] H. Partridge and S. R. Langhoff, *J. Chem. Phys.* **74**, 2361 (1981).
 - [26] M. Brics, J. Rapp, and D. Bauer, *Phys. Rev. A.* **90**, 053418 (2014).
 - [27] C.-Z. Gao, P. M. Dinh, P. Klüpfel, C. Meier, P.-G. Reinhard, and E. Suraud, *Phys. Rev. A.* **93**, 022506 (2016).
 - [28] M. D. Feit, J. A. Fleck, Jr., and A. Steiger, *J. Comput. Phys.* **47**, 412 (1982).
 - [29] R. W. Heather, *Comput. Phys. Commun.* **63**, 446 (1991).
 - [30] I. V. Andrianov and G. K. Paramonov, *Phys. Rev. A.* **59**, 2134 (1999).
 - [31] R. Numico, A. Keller, and O. Atabek, *Phys. Rev. A.* **60**, 406 (1999).